Surface & Coatings Technology 268 (2015) 52–57

Contents lists available at ScienceDirect

Surface & Coatings Technology

journal homepage: www.elsevier.com/locate/surfcoat

Novel opportunities for thermal spray by PS-PVD

G. Mauer [a,*], M.O. Jarligo [a,b], S. Rezanka [a], A. Hospach [a,c], R. Vaßen [a]

[a] Forschungszentrum Jülich GmbH, Institut für Energie- und Klimaforschung (IEK-1), Jülich, Germany
[b] University of Alberta, Department of Chemical and Materials Engineering, Edmonton, Alberta, Canada
[c] Siemens AG, Corporate Technology, Research & Technology Center, München, Germany

ARTICLE INFO

Available online 8 June 2014

Keywords:
Plasma spray-physical vapor deposition
PS-PVD
Microstructure
Thermal barrier coating
Oxygen transport membrane

ABSTRACT

Plasma spray-physical vapor deposition (PS-PVD) is a novel coating process based on plasma spraying. In contrast to conventional methods, deposition takes place not only from liquid splats but also from nano-sized clusters and from the vapor phase. This offers new opportunities to obtain advanced microstructures and thus to comply with the growing demands on modern functional coatings. Thin and dense ceramic coatings as well as highly porous columnar structures can be achieved, offering novel opportunities for the application of thermal spray technology.

This study describes process conditions, which are relevant for the formation of particular microstructures in the PS-PVD process. Following the structure of the process, the feedstock treatment close to the plasma source, plasma particle interaction in the open jet and the formation of coating microstructures on the substrate are covered. Calculated results on the plasma particle interaction under PS-PVD process conditions were found to be in good agreement with OES results and microstructural observations. They show that the feedstock treatment along the very first trajectory segment between injector and jet expansion plays a key role.

Varying the plasma parameters, feedstock treatment can be controlled to a broad extent. Consequently, the manifold nature of the feedstock species arriving on the substrate enables to achieve various coating microstructures. As examples, application specific features of PS-PVD coatings are reported for strain-tolerant thermal barrier coatings as well as for gas-tight oxygen transport membranes with high mixed electronic-ionic conductivity.

1. Introduction

The very low pressure plasma spray (VLPPS) process was developed with the aim of depositing uniform and thin coatings with large area coverage. In comparison to conventional low pressure plasma spraying processes (LPPS, formerly often termed vacuum plasma spraying, VPS) operating at 5–20 kPa, the chamber pressures are typically 50–200 Pa only. VLPPS operates at conventional power level similar to atmospheric plasma spraying (APS) [1,2]. The enhancement of VLPPS by higher electrical input power up to 180 kW led to the development of the LPPS-TF process (TF = thin film). At LPPS-TF conditions, the coating formation still occurs by depositing molten droplets [3] forming highly flowable splats and thus enabling very thin and dense microstructures. Beyond LPPS-TF, it is even possible to evaporate the feedstock material substantially by using specific feedstock powders and process parameters so that nano-sized clusters and condensates from the vapor phase are deposited. Such a process is termed plasma spray-PVD (PS-PVD) [4] and enables advanced microstructures and non-line-of-sight deposition [5,6]. Recent applications are thermal barrier coatings (TBCs) [7,8] and ceramic gas separation membranes [9].

This study describes process conditions, which are relevant for the formation of particular microstructures in the PS-PVD process. Namely columnar-structured strain-tolerant thermal barrier coatings as well as thin and gas-tight oxygen transport membranes with high mixed electronic–ionic conductivity are considered. Following the structure of the process, the feedstock treatment close to the plasma source, the plasma particle interaction in the open jet and the formation of coating microstructures on the substrate are covered.

2. Calculation principles and experimental procedures

Since the conditions between feedstock injection and nozzle exit in the plasma torch are not accessible for measurements, they were estimated by calculation. The principles are reported elsewhere in detail [10]. Plasma gas composition and properties are obtained for chemical equilibrium conditions by finding the minimum Gibbs energy. While doing so, the particular specific enthalpy is assigned to the plasma gas, which results from the net enthalpy flow obtained from the electrical torch input power minus the dissipation energy flow into the cooling water of the torch. The gas dynamics are calculated one-dimensionally assuming an adiabatic and isentropic expansion through the nozzle.

* Corresponding author at: Forschungszentrum Jülich GmbH, Institut für Energie-und Klimaforschung (IEK-1), 52425 Jülich, Germany. Tel.: +49 2461 61 5671; fax: +49 2461 61 2455.
E-mail address: g.mauer@fz-juelich.de (G. Mauer).

http://dx.doi.org/10.1016/j.surfcoat.2014.06.002
0257-8972/

Here, the particular pressure ratio is identified, for which the flow velocity in the critical nozzle section is equal to the local speed of sound. As the plasma gas is highly rarefied, the Knudsen numbers are high. Thus, continuum approaches cannot be applied to calculate the plasma particle interaction. In this study, Chen's methods on the basis on the kinetic theory of gases are used [11–13]. Details on this are reported in [10].

Spray experiments were carried out on a Sulzer Metco Multicoat System (Sulzer Metco, Wohlen, Switzerland). This system is the result of a comprehensive reconstruction of an existing conventional LPPS system. In particular, it was equipped with an additional vacuum pumping unit, a large vacuum blower to provide sufficient pumping capacity at low pressures, enlarged cooling capacity, additional power sources, a new torch transfer system and new control units. In addition to a modified single cathode O3CP torch, which was used in this study, also the F4-VB torch as well as the three-cathode TriplexPro torch can be operated. The two powder injectors positioned opposite each other were located in the cylindrical throat of the O3CP nozzle (D 12.5 mm). A conical part is attached to this critical cross section diverging to the exit cross section (D 19.0 mm).

The plasma characteristics in the expanded jet were investigated by optical emission spectroscopy (OES). Excitation temperatures were determined by the Boltzmann plot method. It is shown below that the plasma is close to local thermal equilibrium (LTE) so that this method is applicable [14]. Electron densities and heavy particle temperatures were calculated by broadening analysis of the H_β hydrogen spectral line belonging to the Balmer series. The details of this procedure are reported elsewhere [15]. The spectrometer applied for OES was an ARYELLE 200 (Laser Technik Berlin (LTB), Berlin, Germany) scanning a wavelength range of 381–786 nm. Plasma radiation was collected through a borosilicate glass window in the process chamber and an achromatic lens, transferred by an optical fiber to the 50 μm entrance slit and detected by a 1024 × 1024 CCD array. The system is equipped with an Echelle grating and the spectral resolution obtained is 15.9–31.8 pm. Calibration was carried out with a spectral Hg lamp.

To obtain the central characteristics of the plasma jet, generally a deconvolution of the measured two-dimensional projections of the integrated intensities must be performed e.g. by Abel inversion to reconstruct the spatial plasma temperature field. However, the differences of the temperatures obtained by Boltzmann plots based on integrated and on de-convoluted intensities were found to be negligibly small. Thus, no de-convolution was performed. In contrast, a method to correct the spectral line broadening [16] yielded substantial corrections of the measured values and was thus applied for broadening analysis.

The first feedstock was an agglomerated 7–8 wt.% yttria partially stabilized zirconia powder (YSZ, Sulzer Metco M6700). A cross section of powder particles is shown in Fig. 1. The characteristic particle sizes measured by laser diffraction were $d_{10} = 2$ μm, $d_{50} = 8$ μm, and $d_{90} =$ 18 μm. Due to the weak agglomeration of this feedstock, immediately after injection into the plasma the particles fragment into small primary particles with dimensions mostly in the sub-micrometer range. Table 1 shows the three plasma spray parameter sets A, B, and C applied for YSZ, which were intended to yield the same plasma net power with three different plasma gas mixtures.

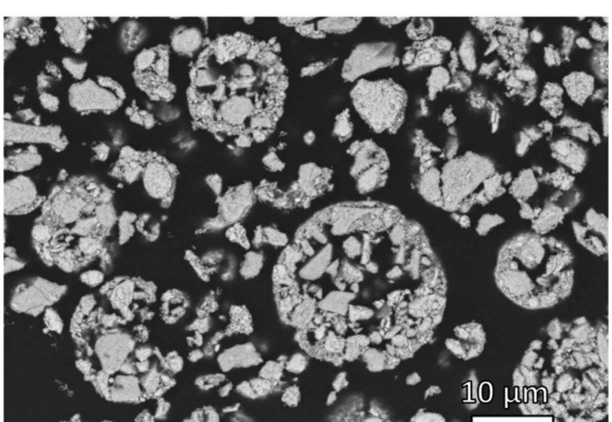

Fig. 1. Cross section of agglomerated 7–8 wt.% yttria partially stabilized zirconia feedstock particles.

The second feedstock material was a rhombohedral perovskite $La_{0.58}Sr_{0.4}Co_{0.2}Fe_{0.8}O_{3-\delta}$ (LSCF, Sulzer Metco D11-4-11). The particles showed a spherical morphology and the characteristic particle sizes measured by laser diffraction were $d_{10} = 6$ μm, $d_{50} = 10$ μm, and $d_{90} = 16$ μm. The powder cut was optimized so that it was fine enough to obtain dense coatings but large enough to be still feedable. The plasma spray parameter set D applied for this material is also given in Table 1. Additional oxygen gas was fed to compensate for the reduction of LSCF.

3. Results and discussion

3.1. Feedstock treatment close to the plasma source

The calculated plasma gas properties are given in Table 2 for the critical and the exit cross section of the nozzle applying the three YSZ process parameters. The hottest conditions prevail for the Ar/He-parameter (A); the Ar/H_2-parameter (C) reveals the lowest temperatures. While the plasma velocities at the critical nozzle cross section cannot exceed the local speed of sound (Mach number Ma = 1), the jet becomes supersonic (Ma > 1) when subsequently passing through the nozzle expansion section. As the flow is faster than the pressure waves traveling in the plasma at the local speed of sound, no information on the chamber pressure is carried inside the nozzle [17]. This means that the plasma gas can exit the nozzle at a pressure, which is higher than the chamber pressure (see pressure values in Table 2).

The plasma gas composition shows the highest ionization degrees for the Ar/He parameter (A) with the highest temperatures. At the critical cross section, more than 70% of the Ar is ionized while He is completely neutral since the temperatures are still too low. At this position, more than 30% of the hydrogen is ionized for parameter B, while it is almost 15% for parameter C only. There is no molecular hydrogen since the temperatures are far above the dissociation level. Knudsen numbers were calculated for a representative spherical particle with a diameter of 1 μm. As they are in the magnitude of 10 and higher, it is evident that the plasma conditions in the nozzle correspond to the free molecular flow regime. Hence, it is advisable to apply Chen's procedures instead of continuum approaches to investigate the plasma particle interaction.

The particle acceleration can be calculated from the particle mass and the drag force. The latter was determined for the critical cross section (=location of the powder injectors) and the nozzle exit (Table 2) and, to simplify matters, assumed to develop linearly in between. The

Table 1
Plasma spray parameters.

Parameter	A	B	C	D
Feedstock	YSZ	YSZ	YSZ	LSCF
Plasma gas	Ar 35 slpm[a] He 60 slpm H_2 –	Ar 35 slpm He 60 slpm H_2 10 slpm	Ar 100 slpm He - H_2 10 slpm	Ar 100–120 slpm He 15–20 slpm H_2 -
Current	2600 A	2200 A	2200 A	2000–2400 A
Net power	60 kW	60 kW	60 kW	55–57 kW
Chamber pressure	200 Pa	200 Pa	200 Pa	200 Pa
Powder feed rate	2×8 g min^{-1}	2×8 g min^{-1}	2×20 g min^{-1}	20 g/min^{-1}
Carrier gas	2 × 16 slpm Ar	2 × 16 slpm Ar	2 × 10 slpm Ar	11 slpm Ar
Spray distance	1000 mm	1000 mm	1000 mm	1000 mm

[a] slpm = standard liters per minute.